The unconventional doping in $YBa_2Cu_3O_{7-x}$/$La_{0.7}Ca_{0.3}MnO_3$ heterostructures by termination control

V. T. Tra, R. Huang, X. Gao, Y.-J. Chen, Y. T. Liu, W. C. Kuo, Y. Y. Chin, H. J. Lin, J. M. Chen, J. M. Lee, J. F. Lee, P. S. Shi, M. G. Jiang, C. G. Duan, J. Y. Juang, C. T. Chen, H. T. Jeng, Q. He, Y.-D. Chuang, J.-Y. Lin, and Y.-H. Chu

Articles you may be interested in

Large tunneling anisotropic magnetoresistance in $La_{0.7}Sr_{0.3}MnO_3$/pentacene/Cu structures prepared on $SrTiO_3$ (110) substrates
Applied Physics Letters **110**, 032401 (2017); 10.1063/1.4974079

Controllable piezoelectricity of $Pb(Zr_{0.2}Ti_{0.8})O_3$ film via in situ misfit strain
Applied Physics Letters **110**, 032901 (2017); 10.1063/1.4974450

Ultra-low coercive field of improper ferroelectric $Ca_3Ti_2O_7$ epitaxial thin films
Applied Physics Letters **110**, 042901 (2017); 10.1063/1.4974217

Room temperature insulating ferromagnetism induced by charge transfer in ultrathin (110) $La_{0.7}Sr_{0.3}MnO_3$ films
Applied Physics Letters **110**, 072405 (2017); 10.1063/1.4976699

Electron radiation damage mechanisms in 2D $MoSe_2$
Applied Physics Letters **110**, 033106 (2017); 10.1063/1.4973809

On the mechanism of highly efficient p-type conduction of Mg-doped ultra-wide-bandgap AlN nanostructures
Applied Physics Letters **110**, 032102 (2017); 10.1063/1.4973999

The unconventional doping in YBa₂Cu₃O₇₋ₓ/La₀.₇Ca₀.₃MnO₃ heterostructures by termination control

V. T. Tra,[1,2] R. Huang,[3,4] X. Gao,[4] Y.-J. Chen,[5,6] Y. T. Liu,[1] W. C. Kuo,[7] Y. Y. Chin,[8] H. J. Lin,[8] J. M. Chen,[8] J. M. Lee,[8] J. F. Lee,[8] P. S. Shi,[1] M. G. Jiang,[1] C. G. Duan,[3] J. Y. Juang,[7] C. T. Chen,[8] H. T. Jeng,[9,10] Q. He,[11] Y.-D. Chuang,[6] J.-Y. Lin,[1,6,a)] and Y.-H. Chu[7,10,12]

[1]*Institute of Physics, National Chiao Tung University, Hsinchu 30010, Taiwan*
[2]*Department of Physics, School of Education, Can Tho University, 3/2 Street, Can Tho, Vietnam*
[3]*Key Laboratory of Polar Materials and Devices, Ministry of Education, East China Normal University, Shanghai 200062, China*
[4]*Nanostructures Research Laboratory, Japan Fine Ceramics Center, Nagoya 456-8587, Japan*
[5]*Department of Physics, National Sun Yat-Sen University, Kaohsiung 80424, Taiwan*
[6]*Advanced Light Source, Lawrence Berkeley National Laboratory, Berkeley, California 94720, USA*
[7]*Department of Electrophysics, National Chiao Tung University, Hshinchu 30010, Taiwan*
[8]*National Synchrotron Radiation Research Center, Hsinchu 30076, Taiwan*
[9]*Department of Physics, National Tsing Hua University, Hsinchu 30043, Taiwan*
[10]*Institute of Physics, Academia Sinica, Taipei 11529, Taiwan*
[11]*Department of Physics, Durham University, Durham DH1 3LE, United Kingdom*
[12]*Department of Materials Science and Engineering, National Chiao Tung University, Hsinchu 30010, Taiwan*

In strongly correlated oxides, heterostructures provide a powerful route to manipulate the charge, spin, orbital, and lattice degrees of freedom to create distinctive functionalities. In this work, we have achieved atomically precise interface control in YBa₂Cu₃O₇₋ₓ/La₀.₇Ca₀.₃MnO₃ (YBCO/LCMO) heterostructures and find a hidden effective doping. This mechanism is responsible for higher T_c in the sample with the MnO₂-terminated interface than in that with the La₀.₇Ca₀.₃O-terminated interface. The MnO₂-terminated sample also shows a larger magnetic moment of Mn together with a lower valence state. For more than a decade, the control of T_c in these heterostructures prior to this work has been solely via the variation of YBCO or LCMO thickness. This work hints at an alternative way of exploiting and exploring the interactions between superconductivity and magnetism in this system. *Published by AIP Publishing.* [http://dx.doi.org/10.1063/1.4973996]

Heterointerfaces between strongly correlated electron systems hold promise for creating multifunctional properties that could not be realized in single-phase bulk materials.[1] Examples are the 2-D electron gas-like behavior at LaAlO₃-SrTiO₃ (STO) interfaces[2,3] and its controllability by a top ferroelectric layer,[4] the emergence of ferromagnetism in a superconducting material at the YBa₂Cu₃O₇₋ₓ/La₀.₇Ca₀.₃MnO₃ (YBCO/LCMO) interface,[5,6] and an induced ferromagnetic state between BiFeO₃ and La₀.₇Sr₀.₃MnO₃ layers.[7,8] Among them, the interface of the YBCO/LCMO heterostructures has been intensively studied to understand the proximity effect between the ferromagnets (F) and superconductors (S).[5,6,9–11] The competition between the ferromagnetic and the superconducting orders leads to a suppression of both their transition temperatures.[12–16] The effects of microstructure imperfection on T_c in this heterostructure were also once discussed.[17] These effects are of topical interest for potential applications in superconducting and magnetoresistance memory devices. The very recent study has further pressed focuses on the selective coupling between Cu, and the peculiar charge density wave (CDW) order in YBCO is found induced by the YBCO/LCMO interface.[18–20] Surprisingly, one key question has yet to be addressed in this prominent YBCO/LCMO system: does the termination type play an important role in

determining the superconducting and magnetic properties? In this work, YBCO/LCMO heterostructures with two distinct types of interfacial terminations are fabricated, and their superconducting and magnetic properties are shown to exhibit different responses to the types of termination. This effective doping through judiciously prepared interfacial terminations, in addition to the widely used thickness control, thus creates an alternative avenue for wider exploitation in electronics devices.

Both YBCO and LCMO have ABO₃ perovskite-related structures. Two possible atomic stacking sequences can be formed along the (001)-oriented heterostructures: (a) La₀.₇Ca₀.₃O-MnO₂-BaO-Cu(II)O₂ (MnO₂-terminated interface, Fig. 1(a)) and MnO₂-La₀.₇Ca₀.₃O-Cu(I)O-BaO-Cu(II)O₂ (La₀.₇Ca₀.₃O-terminated interface, Fig. 1(b)).[21] Realizing this interface design requires atomically precise interface control on the LCMO termination layer, which is achieved by using reflection high-energy electron diffraction (RHEED) assisted pulsed laser deposition (PLD). Two distinct interfaces can be fabricated based on the control of the LCMO termination layer. The details of the heterostructure growth can be found in the supplementary material. In this paper, MnO₂-terminated corresponds to the STO/LCMO₁₀ₙₘ/YBCO_d structure while La₀.₇Ca₀.₃O-terminated corresponds to the STO/SRO₂.₅ᵤ.c./LCMO₁₀ₙₘ/YBCO_d structure. The LCMO layer thickness was fixed to $n = 25$ unit cells (u.c., roughly 10 nm) and the thickness d of YBCO

a)Authors to whom correspondence should be addressed. Electronic addresses: ago@nctu.edu.tw and yhc@nctu.edu.tw

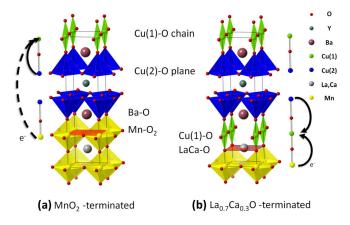**(a)** MnO$_2$-terminated   **(b)** La$_{0.7}$Ca$_{0.3}$O -terminated

FIG. 1. Epitaxial design of heterointerfaces: Schematic of the interfacial control of LCMO/YBCO$_d$ with different interfaces; (a) for the MnO$_2$-terminated interface (La$_{0.7}$Ca$_{0.3}$O-MnO$_2$-BaO-CuO$_2$), the charges are very difficult to transfer because CuO chains are very far from the interface (indicated by a dashed line) while (b) switches into the La$_{0.7}$Ca$_{0.3}$O-terminated (MnO$_2$-La$_{0.7}$Ca$_{0.3}$O-CuO$_2$-BaO) interface by using SRO; electrons transfer easily from LCMO to YBCO due to the CuO chains at the interface (indicated by solid lines).

layer was varied from 2 nm to 100 nm. The SRO layer was inserted to switch the termination of LCMO. This idea was applied to the LCMO/YBCO interface in the present work, though the SRO layer was used to switch the termination of BiFeO$_3$/La$_{0.7}$Sr$_{0.3}$MnO$_3$ before.[22] To confirm the control of these two distinct interfaces, the heterostructures of as-prepared thin films were characterized by high-angle annular dark-field scanning transmission electron microscopy (HAADF-STEM). The HAADF-STEM images of the MnO$_2$-terminated (Fig. 2(a)) and La$_{0.7}$Ca$_{0.3}$O-terminated (Fig. 2(b)) interfaces along the [100] direction clearly show the epitaxial growth of the YBCO layer on top of the LCMO layer with perfectly coherent interfaces in both samples. The intrinsic long period structure of YBCO consisting of an alternation

of two Ba layers and one Y layer, in contrast to the short one of LCMO is clearly observed. To highlight the interface configurations, we have made averaged intensity profiles (see the supplementary material) near the interfaces along the Mn-Cu columns and La$_{0.7}$Ca$_{0.3}$-Ba-Y columns from the raw images. The results corresponding to the MnO$_2$-terminated and La$_{0.7}$Ca$_{0.3}$O-terminated interfaces are shown in Figs. 2(c) and 2(d), respectively. From these intensity profiles, the exact locations of the YBCO/LCMO interfaces are revealed and indicated by the vertical dashed lines. The HAADF-STEM images confirm the atomically sharp interfaces of the YBCO/LCMO heterostructures that are consistent with the schematics as shown in Fig. 1. The samples can then be readily explored on a firm base.

To understand the effects of interfacial termination on the competing orders between YBCO and LCMO, transport measurements were performed from 2 K to room temperature by the standard four-probe method with the electrical contacts on top of YBCO. Figure 3 shows the resistivity $\rho(T)$ of LCMO/YBCO$_d$. Intriguingly, the La$_{0.7}$Ca$_{0.3}$O-terminated samples (red curves) always show a higher value of ρ than the MnO$_2$-terminated samples (black curves), irrespective of the YBCO thickness d. With $d = 6$ nm, the La$_{0.7}$Ca$_{0.3}$O-terminated sample is insulating while the MnO$_2$-terminated sample is superconducting with a transition temperature $T_c = 30$ K (Fig. 3(a)). With the YBCO thickness beyond 6 nm, superconductivity emerges in both the MnO$_2$- and La$_{0.7}$Ca$_{0.3}$O-terminated samples. Figure 3(d) shows that the MnO$_2$-terminated samples consistently have a higher T_c. However, the difference in T_c between MnO$_2$- and La$_{0.7}$Ca$_{0.3}$O-terminated samples is reduced with increased YBCO thickness. An anomaly peak in resistivity is seen in Figs. 3(b) and 3(c) around 170 K as a result of the magnetic transition in the underlying LCMO layer. This anomaly in $\rho(T)$ becomes weaker as the YBCO layer becomes thicker.
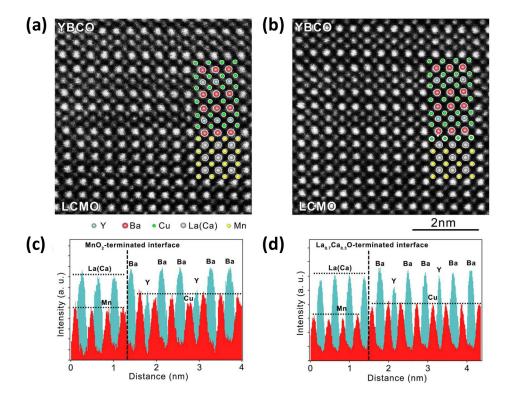

FIG. 2. HAADF-STEM images of the two interfaces along the [100] direction. (a) MnO$_2$-terminated interface. (b) La$_{0.7}$Ca$_{0.3}$O-terminated interface. (c) The averaged intensity profiles along the Mn-Cu columns and La$_{0.7}$Ca$_{0.3}$-Ba-Y columns in (a). (d) The averaged intensity profiles along the Mn-Cu columns and La$_{0.7}$Ca$_{0.3}$-Ba-Y columns in (b). The insets of (a) and (b) are the atomic structures of YBCO and LCMO (only cations are shown). The vertical dashed lines in (c) and (d) indicate the exact locations of the interfaces.
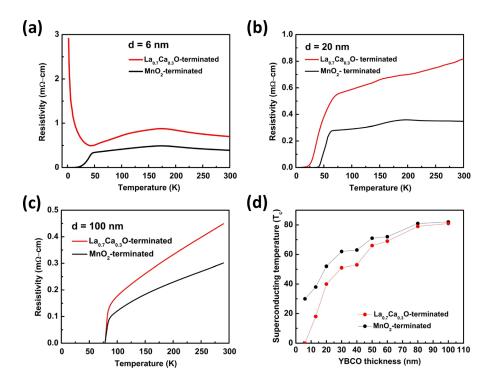
FIG. 3. Transport properties of LCMO/YBCO$_d$ with different interfaces: Resistivity of LCMO/YBCO$_d$ vs. temperature (a) $d = 6\,nm$, (b) $d = 20\,nm$, (c) $d = 100\,nm$, and (d) YBCO thickness dependence of the superconducting transition temperature with either MnO$_2$- or La$_{0.7}$Ca$_{0.3}$O-terminated interfaces.

Different terminations also lead to different magnetic properties in these heterostructures. Figure 4(a) shows the magnetization curves $M(T)$ of LCMO/YBCO$_d$ with a fixed $d = 30\,nm$. Although both samples show similar magnetic transition temperatures, the La$_{0.7}$Ca$_{0.3}$O-terminated sample (red curve) clearly has a smaller magnetization. The $M(H)$ curves of STO/LCMO/YBCO$_{30nm}$ and STO/SRO/LCMO/ YBCO$_{30nm}$ samples were measured by using SQUID at $T = 100\,K$ above T_c to avoid any possible complication from the superconducting state. The data of La$_{0.7}$Ca$_{0.3}$O-terminated sample show a smaller saturation magnetization. To gain insight on these magnetization measurements, we utilized the X-ray absorption spectroscopy (XAS) with

elemental/chemical/orbital specificity. We have recorded the Mn-$L_{2,3}$ XAS spectra and X-ray magnetic circular dichroism (XMCD) with the photon helicity parallel μ^+ (green line) and anti-parallel μ^- (orange line) to the magnetic field. As shown in Fig. 4(c), the XMCD spectra (bottom panel) of LCMO/YBCO$_{2\,nm}$ taken from the difference of the XAS spectra (top panel) with two photon helicities μ^+ and μ^- show the characteristic lineshape of a ferromagnetic Mn atom, and its moment in the La$_{0.7}$Ca$_{0.3}$O-terminated sample is indeed smaller than that in the MnO$_2$-terminated sample. The suppression of the magnetization in the La$_{0.7}$Ca$_{0.3}$O-terminated sample was thus consistently confirmed by both XMCD and SQUID measurements. Figure 4(b) shows the
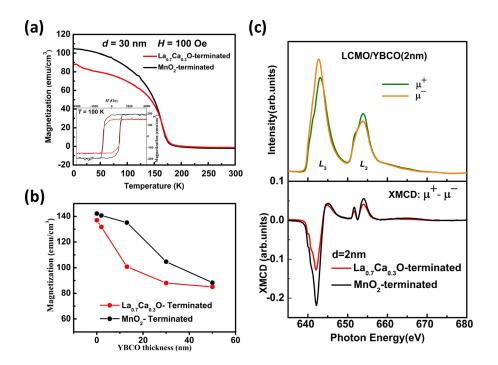

FIG. 4. (a) Temperature dependence of the field cooled magnetization measured in $H = 100\,Oe$ out-of-plane; Inset shows the M-H loops of LCMO/YBCO$_d$ with different interfaces recorded at 100 K and with H applied out-of-plane along [100] STO directions. (b) Low-temperature magnetization as a function of the YBCO layer thickness for two different interfaces. (c) Mn-$L_{2,3}$ spectra of the YBCO (2 nm)/LCMO (10 nm) bilayer with the MnO$_2$-terminated interface taken with circularly polarized X-rays at $T = 30\,K$. The photon spin was aligned parallel (μ^+, green) or anti-parallel (μ^-, orange) to the 1 T magnetic field. The field was applied along the surface normal. A comparison of the normalized Mn-$L_{2,3}$ XMCD signal for YBCO (2 nm)/LCMO(10 nm) with the MnO$_2$-terminated interface (black line) and the La$_{0.7}$Ca$_{0.3}$O-terminated interface (red line) shown in the lower panel.

magnetization as a function of the YBCO thickness. The magnetization in both samples is reduced monotonically with increasing YBCO thickness. $La_{0.7}Ca_{0.3}O$-terminated samples always show a smaller moment. Together with T_c suppression which has been interpreted dominantly due to the proximity effect originating at the LCMO/YBCO$_d$ interfaces,[5,6,10–12] the decreased magnetization is also regarded as being resulted from the competition between ferromagnetism and superconductivity.[13,23–25] However, the F/S competition context alone cannot explain the findings with respect to different interfacial terminations.

XAS further elucidates the valence states of Mn. In Figure 5(a), the Mn K-edge XAS spectra from YBCO/LCMO heterostructures with different interfacial terminations are overlaid with the ones from the standard samples Mn_2O_3 (Mn^{3+}) and MnO_2 (Mn^{4+}). In the K-edge spectra, the energy position of the leading edge can be used to determine the charge valence state. In this figure, it is clear that the $La_{0.7}Ca_{0.3}O$-terminated sample has a higher Mn valence state than the MnO_2-terminated sample. In Figure 5(b), the valence state of Mn for the different terminated samples from different thickness LCMO/YBCO$_d$ ($d = 6$ nm, 10 nm, 13 nm, and 20 nm) heterostructures were plotted as a function of the leading edge energy, with additional data points from reference samples $La_{1-x}Ca_xMnO_3$ ($x = 0$, 0.3, 0.6, and 1). A linear dependence in this plot and the increasing Mn valence state with YBCO thickness in Figs. 5(b) or 5(c) are clear manifestations of the charge redistribution across the interface between the two materials as discussed in the next paragraph. Mn L-edge XAS also strongly support the conclusions from Mn K-edge XAS (see Fig. S2 of the supplementary material). Our results of Mn K-edge XAS represent the bulk-averaged valence state of Mn. It is noted that a very recent study of the interactions between superconducting $La_{1.85}Sr_{0.15}CuO_4$ and ferromagnetic $La_{0.66}Sr_{0.33}MnO_3$ (LSMO) films reveals the variation of Mn valence state over more than 10 unit cells of LSMO.[26]

It is particularly challenging for the conventional F/S competing scenario to reconcile with the simultaneous reduction in T_c and magnetization in the $La_{0.7}Ca_{0.3}O$-terminated samples, because this scenario implies a causal relationship between a larger FM fluctuation and a stronger superconductivity. Neither can the F/S competing scenario explain the direct observations on the change of the Mn valence state in the LCMO layer provided by XAS. On the other hand, previous works have reported the results supporting the charge transfer through the LCMO/YBCO$_d$ interface.[5,27,28] However, the details of such a charge transfer behavior from LCMO to YBCO layer remain unclear. It is found that the range of the corresponding charge redistribution in YBCO due to the distinct types of terminations is beyond the scale of the conventional interface charge transfer. The present observation consequently calls for further mechanisms in addition to the known charge transfer effect. Here we propose a schematic model depicted in Fig. 1. We propose that electrons are redistributed from LCMO to YBCO for both interfacial terminations. Particularly, in $La_{0.7}Ca_{0.3}O$-terminated samples (Fig. 1(b)), CuO chains are much closer to MnO_2 planes in $La_{0.7}Ca_{0.3}O$-terminated samples (Fig. 1(b)) and the relocation of electrons from the
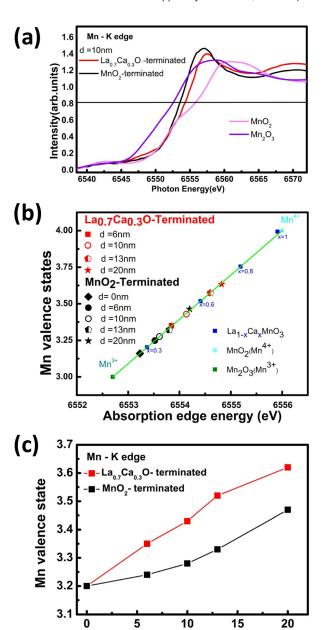

FIG. 5. (a) Mn K-edge XAS spectra of LCMO/YBCO$_d$ with two different interfaces. The YBCO thickness is $d = 10$ nm. Spectra of the Mn_2O_3 (Mn^{3+}) and MnO_2 (Mn^{4+}) standard samples are shown for comparison. All spectra were taken in FY mode. (b) The Mn valence state vs. the absorption edge energy of the MnO_2-terminated (black symbols) and $La_{0.7}Ca_{0.3}O$-terminated (red symbols) samples. $La_{1-x}Ca_xMnO_3$ (where $x = 0$, 0.3, 0.6, and 1) was used as the reference samples, combined with the Mn_2O_3 (Mn^{3+}) and MnO_2 (Mn^{4+}) standard samples to determine the Mn valence state. (c) The Mn valence state as a function of YBCO thickness for two different interfaces.

MnO_2 planes to CuO chains is expected to be relatively more significant (indicated by the black solid arrow). Consequently, the charge transfer from the CuO_2 planes to CuO chains is much suppressed in YBCO, leading to a lower T_c. On comparison, with the MnO_2-terminated interface (Fig. 1(a)), the CuO chains are farther from the MnO_2 planes. Therefore, the tendency for the electrons to move from MnO_2 planes to CuO chains is weaker (indicated by the black dashed arrow). This effective doping mediated by the interface can be the first order interaction as important as the short length scale interaction (charge transfer and

magnetic competition). How this interface-related mechanism induces a long range effective doping remain elusive. Therefore, we investigate this issue using first-principles calculations. The first principles calculations indeed reveal the effective doping occurring both in YBCO and LCMO that may explain the observed superconducting, transport and magnetic properties of the YBCO/LCMO heterostructures. (For details of the calculations and results, see Fig. S3 of the supplementary material)

The effective doping reported in the present work, while in agreement with the previous reports,[27,29–32] might not be totally inconsistent with the recent claim of short-range charge transfer at the interfaces.[28] They are merely different findings revealed by different probes. Mechanisms like coupling of charge and orbital degrees of freedom, strain field, long-range electron-phonon coupling induced by the combination of Coulomb force and short-range orbital reconstruction proposed in Ref. 28. may be in place to extend the effects of the distinct interfaces throughout the entire YBCO slab. The present scenario might also be related to the recently found CDW with a long range order.[19,20] Our data clearly provide another degree of freedom to effectively manipulate the superconducting and physical properties in these heterostructures.

To conclude, the findings in the present work would have been impossible without an atomically precise interface control. We have shown that the interface has played a more prominent role than previously thought on affecting the magnetic and electronic properties of F/S heterostructures. This effective doping effect due to the types of the interfaces is tremendously important for understanding these heterostructures. Moreover, this study opens another avenue to design and engineer the functional oxide interfaces.

See supplementary materials for experimental details and the supporting results of XAS, TEM, and first principles calculations.

[1] H. Y. Hwang, Y. Iwasa, M. Kawasaki, B. Keimer, N. Nagaosa, and Y. Tokura, Nat. Mater. **11**, 103 (2012).

[2] A. Ohtomo and H. Y. Hwang, Nature **427**, 423 (2004).

[3] J. Biscaras, N. Bergeal, A. Kushwaha, T. Wolf, A. Rastogi, R. C. Budhani, and J. Lesueur, Nat. Commun. **1**, 89 (2010).

[4] V. T. Tra, J. W. Chen, P. C. Huang, B. C. Huang, Y. Cao, C. H. Yeh, H. J. Liu, E. A. Eliseev, A. N. Morozovska, J.-Y. Lin, Y. C. Chen, M. W. Chu,

[5] P. W. Chiu, Y. P. Chiu, L. Q. Chen, C. L. Wu, and Y.-H. Chu, Adv. Mater. **25**, 3357 (2013).

[6] J. Chakhalian, J. W. Freeland, G. Cristiani, H.-U. Habermeier, G. Khaliullin, M. Van Veenendaal, and B. Keimer, Science **318**, 1114 (2007).

[7] J. Chakhalian, J. W. Freeland, G. Srajer, J. Strempfer, G. Khaliullin, J. C. Cezar, T. Charlton, R. Dalgliesh, C. Bernhard, G. Cristiani, H.-U. Habermeier, and B. Keimer, Nat. Phys. **2**, 244 (2006).

[8] P. Yu, J.-S. Lee, S. Okamoto, M. D. Rossell, M. Huijben, C.-H. Yang, Q. He, J. X. Zhang, S. Y. Yang, M. J. Lee, Q. M. Ramasse, R. Erni, Y.-H. Chu, D. A. Arena, C.-C. Kao, L. W. Martin, and R. Ramesh, Phys. Rev. Lett. **105**, 027201 (2010).

[9] S. M. Wu, S. A. Cybart, P. Yu, M. D. Rossell, J. X. Zhang, R. Ramesh, and R. C. Dynes, Nat. Mater. **9**, 756 (2010).

[10] C. A. R. Sa de Melo, Phys. Rev. Lett. **79**, 1933 (1997).

[11] V. Peña, C. Visani, J. Garcia-Barriocanal, D. Arias, Z. Sefrioui, C. Leon, J. Santamaria, and C. A. Almasan, Phys. Rev. B **73**, 104513 (2006).

[12] J. Stahn, J. Chakhalian, Ch. Niedermayer, J. Hoppler, T. Gutberlet, J. Voigt, F. Treubel, H.-U. Habermeier, G. Cristiani, B. Keimer, and C. Bernhard, Phys. Rev. B **71**, 140509 (2005).

[13] S. Soltan, J. Albrecht, and H.-U. Habermeier, Phys. Rev. B **70**, 144517 (2004).

[14] Z. Sefrioui, D. Arias, Z. Sefrioui, V. Peña, J. E. Villegas, M. Varela, P. Prieto, C. León, J. L. Martinez, and J. Santamaria, Phys. Rev. B **67**, 214511 (2003).

[15] E. Dagotto, Science **318**, 1076 (2007).

[16] J. Hoppler, J. Stahn, Ch. Niedermayer, V. K. Malik, H. Bouyanfif, A. J. Drew, M. Rössle, A. Buzdin, G. Cristiani, H. U. Habermeier, B. Keimer, and C. Bernhard, Nat. Mater. **8**, 315 (2009).

[17] Z. L. Zhang, U. Kaiser, S. Soltan, H. U. Habermeier, and B. Keimer, Appl. Phys. Lett. **95**, 242505 (2009).

[18] H. Zhang, N. Gauquelin, G. A. Botton, and J. Y. T. Wei, Appl. Phys. Lett. **103**, 052606 (2013).

[19] S. W. Huang, L. Andrew Wray, H.-T. Jeng, V. T. Tra, J. M. Lee, M. C. Langner, J. M. Chen, S. Roy, Y. H. Chu, R. W. Schoenlein, Y.-D. Chuang, and J.-Y. Lin, Sci. Rep. **5**, 16690 (2015).

[20] J. He, P. Shafer, T. R. Mion, V. T. Tra, Q. He, J. Kong, Y.-D. Chuang, W. L. Yang, M. J. Graf, J.-Y. Lin, Y.-H. Chu, E. Arenholz, and R.-H. He, Nat. Commun. **7**, 10852 (2016).

[21] A. Frano, S. Blanco-Canosa, E. Schierle, Y. Lu, M. Wu, M. Bluschke, M. Minola, G. Christiani, H. U. Habermeier, G. Logvenov, Y. Wang, P. A. v. Aken, E. Benckiser, E. Weschke, M. Le Tacon, and B. Keimer, Nat. Mater. **15**, 831 (2016).

[21] M. Varela, A. R. Lupini, S. J. Pennycook, Z. Sefrioui, and J. Santamaria, Solid-State Electron. **47**, 2245 (2003).

[22] P. Yu, W. Luo, D. Yi, J. X. Zhang, M. D. Rossell, C. H. Yang, L. You, G. S. Bhalla, S. Y. Yang, Q. He, Q. M. Ramasse, R. Erni, L. W. Martin, Y.-H. Chu, S. T. Pantelides, S. J. Pennycook, and R. Ramesh, Proc. Natl. Acad. Sci. U.S.A. **109**, 9710 (2012).

[23] H. U. Habermeier, J. Phys.: Conf. Ser. **108**, 012039 (2008).

[24] J. Salafranca and S. Okamoto, Phys. Rev. Lett. **105**, 256804 (2010).

[25] C. B. Cai, L. Peng, B. Holzapfel, X. M. Xie, Z. Y. Liu, Y. M. Lu, and C. Z. Chen, Supercond. Sci. Technol. **23**, 034010 (2010).

[26] G. M. De Luca, G. Ghiringhelli, C. A. Perroni, V. Cataudella, F. Chiarella, C. Cantoni, A. R. Lupini, N. B. Brookes, M. Huijben, G. Koster, G. Rijnders, and M. Salluzzo, Nat. Commun. **5**, 5626 (2014).

[27] T. Holden, H. U. Habermeier, G. Cristiani, A. Golnik, A. Boris, A. Pimenov, J. Humlcek, O. I. Lebedev, G. Van Tendeloo, B. Keimer, and C. Bernhard, Phys. Rev. B **69**, 064505 (2004).

[28] T. Y. Chien, L. F. Kourkoutis, J. Chakhalian, B. Gray, M. Kareev, N. P. Guisinger, D. A. Muller, and J. W. Freeland, Nat. Commun. **4**, 2336 (2013).

[29] C. T. Chen, L. H. Tjeng, J. Kwo, H. L. Kao, P. Rudolf, F. Sette, and R. M. Fleming, Phys. Rev. Lett. **68**, 2543 (1992).

[30] Y.-J. Chen, M. G. Jiang, C. W. Luo, J.-Y. Lin, K. H. Wu, J. M. Lee, J. M. Chen, Y. K. Kuo, J. Y. Juang, and C. Y. Mou, Phys. Rev. B **88**, 134525 (2013).

[31] J. Salafranca, J. Rincn, J. Tornos, C. Len, J. Santamaria, E. Dagotto, S. J. Pennycook, and M. Varela, Phys. Rev. Lett. **112**, 196802 (2014).

[32] N. Driza, S. B. Canosa, M. Bakr, S. Soltan, M. Khalid, L. Mustafa, K. Kawashima, G. Christiani, H. U. Habermeier, G. Khaliullin, C. Ulrich, M. Le Tacon, and B. Keimer, Nat. Mater. **11**, 675 (2012).